ground water

Sea Water Intrusion by Sea-Level Rise: Scenarios for the 21st Century

by Hugo A. Loáiciga[1], Thomas J. Pingel[2], and Elizabeth S. Garcia[2]

Abstract

This study presents a method to assess the contributions of 21st-century sea-level rise and groundwater extraction to sea water intrusion in coastal aquifers. Sea water intrusion is represented by the landward advance of the 10,000 mg/L iso-salinity line, a concentration of dissolved salts that renders groundwater unsuitable for human use. A mathematical formulation of the resolution of sea water intrusion among its causes was quantified via numerical simulation under scenarios of change in groundwater extraction and sea-level rise in the 21st century. The developed method is illustrated with simulations of sea water intrusion in the Seaside Area sub-basin near the City of Monterey, California (USA), where predictions of mean sea-level rise through the early 21st century range from 0.10 to 0.90 m due to increasing global mean surface temperature. The modeling simulation was carried out with a state-of-the-art numerical model that accounts for the effects of salinity on groundwater density and can approximate hydrostratigraphic geometry closely. Simulations of sea water intrusion corresponding to various combinations of groundwater extraction and sea-level rise established that groundwater extraction is the predominant driver of sea water intrusion in the study aquifer. The method presented in this work is applicable to coastal aquifers under a variety of other scenarios of change not considered in this work. For example, one could resolve what changes in groundwater extraction and/or sea level would cause specified levels of groundwater salinization at strategic locations and times.

Introduction

The California Department of Water Resources (CDWR) issued a landmark report in July 2006 that incorporated climate change predictions into management of California's water resources (CDWR 2006). The CDWR identified saline intrusion into coastal aquifers as one likely impact of modern-age climate change. Although sea level has been rising since the end of the last (Wisconsinan) Ice Age, the rate of increase might have been recently exacerbated by thermal expansion and ice melting caused by anthropogenic greenhouse gas (GHG) emissions to the atmosphere (Intergovernmental Panel for Climate Change—IPCC 2007). Other effects of increased GHGs emissions, CO_2, specifically, on sea water have been pondered in Loáiciga (2006, 2007).

Global mean sea level (GMSL) increased by an average rate of 1.8 mm/year during the 20th century (Douglas 1997). The IPCC (2007) reports a high confidence that this rate has been increasing (see, also, Bates et al. 2008). The IPCC estimated that GMSL increased 3.1 mm/year from 1993 to 2003, although this change is not spatially uniform worldwide. Nicholls and Cazenave (2010) estimated a GMSL rise of approximately 3.3 mm/year in the period 1992 to 2010. The rise of sea level poses exacerbated threats in coastal aquifers undergoing land subsidence and decreased riverine sediment output to estuaries (Anderson et al. 2010; Nicholls and Cazenave 2010), while its threat is diminished in pre-glaciated areas undergoing isostatic rebound. Eight long-term tidal records on the coast of

[1]Corresponding author: Department of Geography, University of California, Santa Barbara, CA 93106; (805) 450 4432; fax (805) 308 2578; hugo@geog.ucsb.edu

[2]Department of Geography, University of California, Santa Barbara, CA 93106.

Received July 2010, accepted January 2011.

doi: 10.1111/j.1745-6584.2011.00800.x

California exhibit increases in mean sea level (MSL) ranging from 0.84 mm/year (Los Angeles) to 2.22 mm/year (La Jolla), while one station shows a decrease in MSL of −0.48 mm/year (CDWR 2006) during the 20th century.

The CDWR (2006) postulated an increase in sea level ranging from 0.10 to 0.90 m along California's coast during the 21st century, which is consistent with recent 21st-century predictions of GMSL by Nicholls and Cazenave (2010). One effect of such an increase in sea-level rise is to induce sea water intrusion into coastal aquifers (Bear et al. 1999; Masterton and Garabedian 2007; Werner and Simmons 2009). Sea water intrusion caused by groundwater extraction has been noted in Monterey, Santa Cruz, and Ventura counties of California, and in lands surrounding the San Francisco Bay, dating back to the 1930s, as well as in many other parts of the world (Bear et al. 1999; Zektser et al. 2005; Loáiciga 2008). Groundwater has a prominent role in water supply in California—accounting to about 40% of its urban and agricultural water use (Bachman et al. 2005; CDWR 2009)—thus the concern to address the threat posed by future sea-level rise to California's coastal aquifers. Similar concerns apply to coastal aquifers in other regions given that more than 60% of the world population lives within 30 km of oceanic shorelines.

Although sea water intrusion into coastal aquifers is a long-studied problem (Ghyben 1888; Herzberg 1901), the relatively recent development of advanced numerical models has enabled in-depth three-dimensional modeling of fresh water-sea water interactions at specific sites (Yeh and Bray 2006; Bray et al. 2007; Kumar et al. 2007). FEFLOW is one such numerical modeling software system capable of accounting for density-dependent solute transport (Diersch 2006; Trefrey and Muffels 2007) and, thus, appropriate for simulating sea water intrusion in coastal aquifers caused by natural and anthropogenic processes. There have been several recent uses of FEFLOW to model sea water intrusion into coastal aquifers. Faye et al. (2001) modeled sea water intrusion into a confined aquifer in Senegal. Kumar et al. (2007) modeled sea water intrusion using a seven-layer FEFLOW model. Barazzuoli et al. (2008) used FEFLOW to model sea water intrusion caused by pumping near the coastal production wells. An exhaustive literature review of sea-level rise and sea water intrusion is beyond the scope of this work. Bear et al. (1999) reviewed several numerical models with sea water intrusion simulation capabilities, including SHARP, SUTRA, HST3D, MOCDENS3D, and an early version of FEFLOW. Loáiciga (2003a) reported a methodology to assess the impacts of climate change and groundwater extraction on aquifer recharge and springflow.

This article presents a method for assessing the contributions of 21st-century sea-level rise and groundwater extraction to sea water intrusion in coastal aquifers. A general mathematical formulation of the resolution of sea water intrusion among its causes has been formulated via numerical simulation under key scenarios of change: (1) 21st-century groundwater extraction and 1 m (or other) sea-level rise; (2) baseline groundwater extraction and 1 m (or other) sea-level rise; and (3) 21st-century groundwater extraction and baseline sea level. The method is illustrated with numerical simulations of sea water intrusion in the Seaside Area (groundwater) sub-basin of the Salinas Valley Groundwater Basin of Monterey County, California. The Seaside sub-basin features relatively high topographic relief, steep groundwater gradients toward the ocean, unconfined flow, and relatively simple stratigraphy (Muir 1982; CDWR 2003).

Method for Assessing the Contributions of Sea-Level Rise and Groundwater Extraction to Sea Water Intrusion

Sea water intrusion is measured in this work by the landward advance of the 10,000 mg/L iso-salinity line (measured from the coastline defined by a baseline sea level defined in the section "Elevation Datums and Coordinate Systems"), a concentration of salts that renders groundwater unsuitable for human use (U.S. Environmental Protection Agency 1976). Because the position of the 10,000 mg/L iso-salinity line differs across the landscape, its leading position landward was chosen as the primary variable of analysis herein. Let the advance of sea water intrusion so defined be denoted by $f(Q, R)$, where f is a function of sea-level rise (R) and groundwater extraction (Q). Let $R = R_0$ denote the baseline sea level from which future rise in sea level is measured and $Q = Q_0$ be the baseline groundwater extraction relative to which future groundwater is measured. The baseline sea water intrusion is $f(Q_0, R_0)$. If the function f were known, the change in sea water intrusion (Δf_{Q+R}) caused by a change in groundwater extraction ($Q = Q_0 + \Delta Q$) and a change in sea-level rise ($R = R_0 + \Delta R$) would be:

$$\Delta f_{Q+R} = f(Q, R) - f(Q_0, R_0) \tag{1}$$

A change in sea water intrusion caused by changed sea-level rise while groundwater extraction remains at its baseline Q_0 would be:

$$\Delta f_R = f(Q_0, R) - f(Q_0, R_0) \tag{2}$$

Sea water intrusion effected by a change in groundwater extraction while sea level is fixed at R_0 is given by:

$$\Delta f_Q = f(Q, R_0) - f(Q_0, R_0) \tag{3}$$

It can be shown that the sum of Equations 2 and 3, $\Delta f_R + \Delta f_Q$, approximates Equation 1 (Δf_{Q+R}) well if the function f is nearly linear on Q and R. In this instance, Equations 2 and 3 approximate the contributions to sea water intrusion caused by sea-level rise and groundwater extraction, respectively. Loáiciga (2003a) demonstrated that the linear approximation was reasonable for estimating the relative effects of changes in groundwater recharge by climate change and of groundwater extraction in a large regional aquifer.

In actuality, the function f is unknown, and one must approximate the formulas shown in Equations 1 through 3 numerically. For example, in the case of Equation 1, one states that the baseline or initial condition for the function f, or $f(Q_0, R_0)$, corresponds to sea water intrusion in which sea-level rise and groundwater extraction equal their baseline levels. Thereafter, sea water intrusion caused by changed sea level ($R = R_0 + \Delta R$) and changed groundwater extraction ($Q = Q_0 + \Delta Q$) is calculated by numerical simulation. The calculated sea water intrusion caused by Q and R minus that caused by Q_0 and R_0 approximates Equation 1.

The approximation of Equations 2 and 3 is handled in an analogous manner. For example, the numerical approximation to Equation 2 is accomplished by calculating sea water intrusion caused by sea-level rise ($R = R_0 + \Delta R$) with groundwater fixed at its baseline level ($Q = Q_0$). The calculated sea water intrusion minus that caused by Q_0 and R_0 approximates Equation 2.

Other impact scenarios can be resolved by strategic simulation of sea water intrusion driven by groundwater extraction and/or sea-level rise. Suppose, for example, that a certain amount of future groundwater extraction (Q) is calculated to produce sea water intrusion $f(Q, R_0) - f(Q_0, R_0)$ and that one is interested in finding the sea-level rise that would produce the same level of sea water intrusion if groundwater extraction were kept at its baseline level Q_0. It follows from Equations 2 and 3 that one must find (by numerical simulation) the value of sea-level rise R^* such that it satisfies the following equation:

$$f(Q_0, R^*) = f(Q, R_0) \tag{4}$$

The solution to Equation 4 may or may not yield a physically meaningful value of sea-level rise R^*. That is, the required R^* may exceed the realm of physically-realizable sea level within a practical time horizon (say, 100 years). Excessive sea-level rise poses primarily problems related to flood control.

The following sections contain an application of this section's method.

Physiographic Description of the Seaside Area Sub-Basin

The Seaside Area sub-basin is part of the large Salinas Valley Groundwater Basin of Monterey County, California. The sub-basin, as modeled, is approximately 6038 ha in area. The hydrogeologic setting of the Seaside Area sub-basin was described in detail by Muir (1982). Figure 1 shows a location map for the Seaside Area sub-basin and its geographical boundaries. The "Hydrogeology of the Seaside Area Sub-Basin" section contains a brief hydrostratigraphic description of the Seaside Area sub-basin.

The coastal Seaside Area sub-basin receives an average 43 cm of rain per year, whereas the inland areas receive approximately 38 cm of rain annually (CDWR 2003). The sub-basin lies northwest/southeast

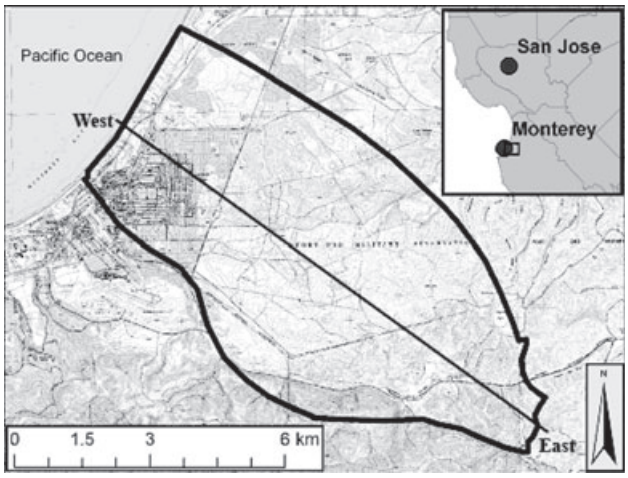

Figure 1. Seaside Area groundwater sub-basin, near Monterey, California. The West-East elevation cross section is shown in Figure 4.

with groundwater generally flowing from the southeastern foothills (150 to 250 m in elevation near the sub-basin boundary) to the sea. The urban area connected to the city of Seaside is largely concentrated near the southern portion of the coastal section. According to census figures, the city of Seaside had a population of some 33,500 people in 2007, a number largely unchanged since 1990.

The bulk of the sub-basin is occupied by the Fort Ord Military Reservation, which closed as an active duty base in 1994. As a result, the greater area of the sub-basin is undeveloped with the exception of several ranches along the southern border. There are only a few small streams within the basin, with most surface drainage occurring into small depressions (CDWR 2003). Vegetation is generally coastal scrub and chaparral throughout the area (Yates et al. 2005).

The tidal monitoring station in the City of Monterey (near the Seaside sub-basin) shows an average annual sea-level rise of 1.34 mm based on online data from 1973 to 2008 (National Oceanic and Atmospheric Administration—NOAA 2009).

Historical Groundwater Extraction in the Seaside Area Sub-Basin

Yates et al. (2005) reported that while there are 20 active groundwater extraction wells in the sub-basin, nearly all water (99%) comes from 13 of these wells, whose depths vary from 50 to 200 m. These wells are spatially concentrated within 3 km of the coast. Although Muir (1982) reported an average annual groundwater extraction of 4.44×10^6 m^3 ($\cong$12,160 m^3/d), the average annual extraction from 1995 to 2005 was 5.50×10^6 m^3 ($\cong$15,070 m^3/d). Yates et al. (2005) calculated the mean total annual extraction for 2002 to 2006 as approximately 5.60×10^6 m^3 ($\cong$15,340 m^3/d). Figure 2 shows the increase in total production from the 20 historically

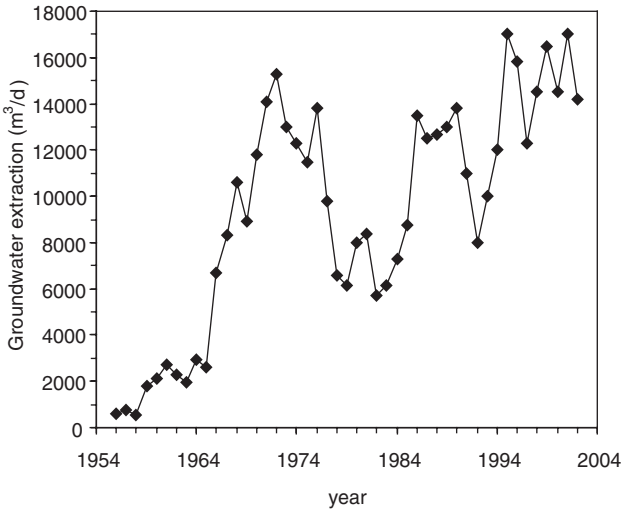

Figure 2. Groundwater extraction from historically most active wells since 1956 for Seaside Area sub-basin (Durbin 2007).

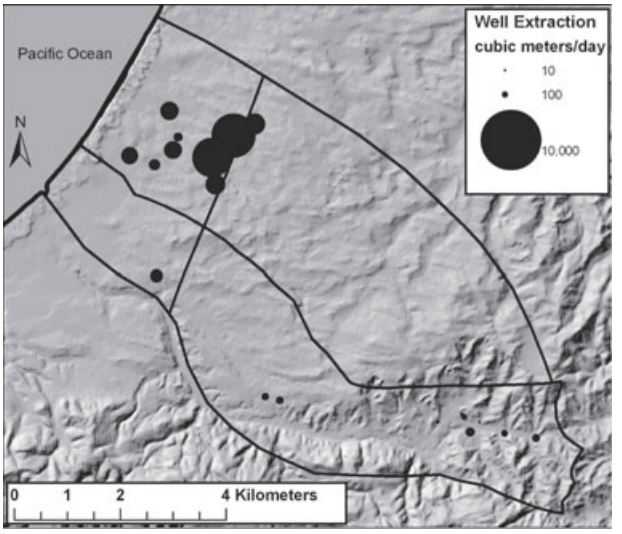

Figure 3. Proportional circle map of well location and groundwater extractions rates based on information in Yates (2005). The Seaside Area sub-basin is divided into four areas delimited by the black solid lines.

most active wells since 1956 (assembled from historical data presented by Durbin 2007).

Contention over groundwater pumping between commercial, municipal, and private users led to a Court-appointed Water Master for the Seaside Area groundwater sub-basin. The Water Master is tasked with acting as arbiter between all parties and setting limits on groundwater extraction. Decreasing groundwater levels (Muir 1982; Yates et al. 2005; Durbin 2007), particularly a below-sea-level depression near the coastal production wells, prompted the Water Master to aim for a level of extraction or operating yield that is consistent with the sub-basin's sustainable yield. Yet, this aim has proven elusive, because the sustainable yield has not been determined with certainty. Yates et al. (2005) estimated the total sustainable (annual) yield at 3.55×10^6 m^3 ($\cong$9730 m^3/d), though uncertainty surrounds this estimate (see Loáiciga 2003b for a review of groundwater sustainability). The extraction imbalance, or overdraft, whereby groundwater pumping exceeds recharge, has been mitigated to some extent by the introduction of two injection wells near the coast. These two wells accounted for 628 m^3/d of water injected. However, groundwater levels near the coast have been in steady decline since at least 1982 (Muir 1982) at a rate of 0.2 to 0.3 m per year (Yates et al. 2005). As of 2006, there are cones of depression surrounding the largest production wells about 2.5 km from the coast.

Figure 3 shows the spatial location of the current extraction using proportional circles to denote the amount of groundwater extracted. Due to differences in land cover, land use, and rainfall, Yates et al. (2005) divided the Seaside sub-basin into four subareas, which are shown in Figure 3. Nearly all groundwater in the sub-basin is extracted from the Northern Coastal subarea, and no groundwater is extracted from the Northern Inland subarea. Most water extracted is for urban use, although some is used for agriculture and golf courses (CDWR 2003).

Hydrogeology of the Seaside Area Sub-Basin

The study area has four main groundwater-bearing formations underlain by Monterey shale on the bottom, which acts as a no-flow boundary (Muir 1982; Fugro West Inc. 1997; Yates et al. 2005), as shown on the elevation cross section depicted in Figure 4. The bottommost layer is the Santa Margarita Formation and consists of poorly consolidated marine sandstone. On top of this lies the Paso Robles Formation, which is also largely sandstone with some clay and gravel. Overlaid on the Paso Robles Formation are poorly consolidated dune sand deposits in some areas. The fourth formation, the Aromas Formation, is typically grouped with either the Paso Robles or semi-consolidated dune sand deposits due to similarity in lithology. The aquifer system thickness varies, as shown in Figure 4. In general, the aquifer system is thickest to the north, and thins substantially toward the south. There is no barrier to flow between the main water-bearing formations (Muir 1982), which exhibit similar lithology and a relatively narrow range of hydraulic conductivity. Yates et al. (2005) estimated hydraulic conductivity to vary from 0.5 to 1.5 m/d based on numerical model calibrations. The range of variation of hydraulic conductivity in the Seaside sub-basin is relatively small when compared with those of more heterogeneous formations. Hydraulic conductivity in highly heterogeneous formations varies over several orders of magnitude (see an example of this type of variability in the clayey formations underlying Mexico City, Loáiciga et al. 2006). Further details about estimated aquifer parameters in the Seaside Area sub-basin are given in the section "Aquifer Parameter Specification."

Recharge varies across the four subareas into which the Seaside Sub-basin is divided, shown in Figure 3 (Durbin 2007): Northern Coastal = 0.401 mm/d, Southern Coastal = 0.309 mm/d, Northern Inland = 0.175 mm/d, and Southern Inland (Laguna Seca) = 0.223 mm/d.

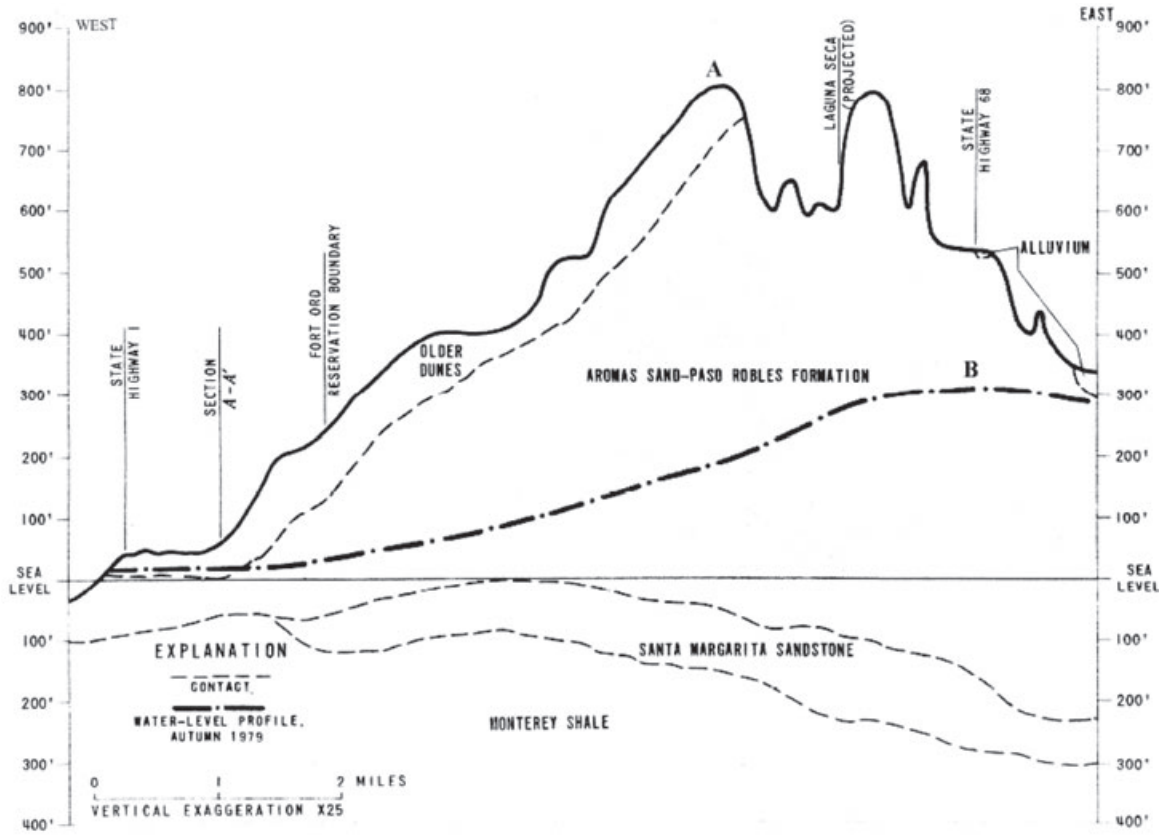

Figure 4. A simplified cross section showing the key features of the Seaside Area sub-basin's hydrostatigraphy. The outline of this West-East section is depicted in Figure 1. Vertical scale in feet (1 foot = 0.3048 m). Horizontal scale in miles (1 mile = 1609 m). After Muir (1982).

The overall spatially-weighted mean recharge for the Seaside sub-basin equals 0.231 mm/d, which is close to the value 0.210 mm/d used by Durbin (2007).

Summary of the Numerical Model

A three-dimensional, finite-element model of the Seaside Area sub-basin was constructed using the FEFLOW software package, version 5.3 (Diersch 2006). FEFLOW is a numerical, coupled, groundwater flow-solute transport-heat numerical simulation model. FEFLOW uses a finite-element spatial grid, giving it unique capabilities to represent accurately the geographical layout of an aquifer, this being a substantial geometric advantage over alternative finite-difference models. Figure 5 shows a plan view of the finite-element mesh for the Seaside Area sub-basin. The model allows time-dependent and spatially variable recharge, pumping, injection, and boundary conditions. The mathematical equations of flow and solute transport solved by FEFLOW in this study (after discretization in a finite-element grid) are given as follows:

Groundwater flow equation (Diersch 2006; see, also, Langevin and Guo 2006):

$$\nabla\cdot\left[\rho\frac{\mu_f}{\mu}K_f\left(\nabla h+\frac{\rho-\rho_f}{\rho_f}\nabla z\right)\right]=\rho S_f\frac{\partial h}{\partial t}+\Phi\frac{\partial\rho}{\partial C}\frac{\partial C}{\partial t} \quad (5)$$

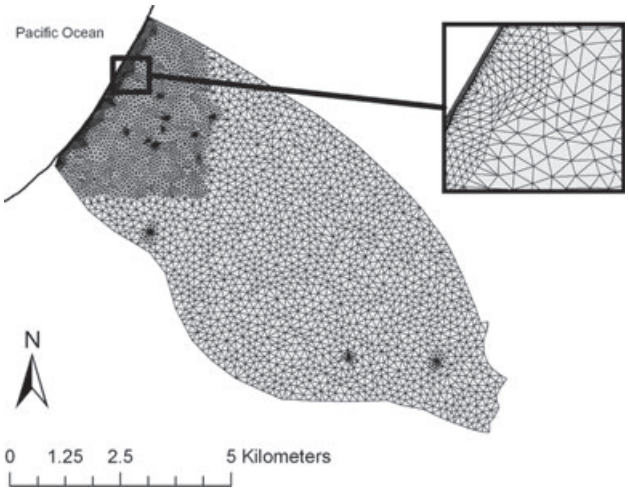

Figure 5. Triangular finite-element mesh for the Seaside Area sub-basin. Notice the finer spatial resolution used near the coastline.

in which ρ = density of saline groundwater; ρ_f = the density of fresh groundwater ($\sim$1000 kg/m^3); μ = dynamic viscosity of saline groundwater; μ_f = dynamic viscosity of fresh groundwater; z = elevation head; ϕ = porosity; S_f = specific storage of fresh groundwater; C = the concentration of dissolved salts (or salinity) in

groundwater; h = fresh water equivalent hydraulic head; t = the time variable; ∇ = the gradient operator in three-dimensional, Cartesian, coordinates; K_f = hydraulic conductivity of fresh groundwater, where $K_f = k\rho_f g/\mu_f$, k = permeability, g = acceleration of gravity.

Solute transport equation (Diersch 2006; see, also, Langevin and Guo 2006):

$$\frac{\partial \phi C}{\partial t} = \nabla\cdot(\phi D\cdot\nabla C) - \nabla\cdot(\boldsymbol{q}C) \qquad (6)$$

in which D = hydrodynamic dispersion tensor, $\boldsymbol{q}$ = vector of Darcian fluxes of groundwater, and all other variables are defined after Equation 5. See the section "Aquifer Parameter Specification" for information on aquifer parameters used in the numerical simulation model.

In addition, there are empirical equations relating the density ρ and (dynamic) viscosity μ to salinity, pore pressure, and water temperature (see Diersch 2006). Equations 5 and 6, together with the empirical equations for density and viscosity, are discretized via the finite-element method and solved numerically in FEFLOW (see Diersch 2006).

Elevation Datums and Coordinate Systems

One critical aspect of modeling sea-level rise is to obtain proper geodetic representation of what "MSL" is and to ensure that aquifer topography is properly related to the correct MSL to avoid errors introduced by inaccurate vertical control. Most of the existing geographical data used were originally in the State of California Plane Coordinate System (California Zone IV) and used the National Geodetic Vertical Datum of 1929 (NGVD29) and the North American Datum of 1927. These were reprojected into the Universal Transverse Mercator (Zone 11N) coordinate system, North American Vertical Datum of 1988 (NAVD88), and the World Geodetic System of 1984. Data were also typically provided in the U.S. customary system of units and were converted to their respective metric values. As the impact of MSL was a principal variable of interest for this study, it was crucial to accurately relate the various vertical datums (e.g., MSL and its near-approximations) at the coast. NOAA provides online data calculated from coastal benchmarks. According to these data, for the epoch 1983 to 2001, the vertical datums are related as shown in Table 1 (National Geodetic Survey 2009).

The "zero" mark for our models corresponded to the NAVD88 datum. As a result, year 2006 sea level was modeled as 0.903 m above this datum, this being the initial condition for sea level, that is, $R_0 = 0.903$ m.

Table 1
Relationship of Vertical Datums Near Seaside, California (Station ID 9413450, PID GU2090)

Datum	Height (m)
Mean higher high water (MHHW)	1.667
Mean high water (MHW)	1.453
Mean sea level (MSL)	**0.903**
National Geodetic Vertical Datum of 1929 (NGVD29)	0.833
Mean low water (MLW)	0.374
Mean lower low water (MLLW)	0.041
North American Vertical Datum of 1988 (NAVD88)	0.000

Note: The NAVD88 was the chosen vertical datum, so that the mean sea level (MSL) equaled 0.903 m in 2006.

Model Boundaries, Finite-Element Mesh, and Groundwater Extraction

Model boundaries of the Seaside Area sub-basin were initially defined by Muir (1982) and refined by Yates et al. (2005) and are shown in Figure 1, previously discussed in the section "Physiographic Description of the Seaside Area Sub-Basin." These boundaries were supplied to the authors by the Monterrey Peninsula Water Management District (Sandoval 2008). The total size of the basin, as modeled, was 6038 ha. The southwest (no-flow) boundary was derived from the Chupines fault location where uplifted Monterey shale formation prevents groundwater from flowing (Muir 1982). The eastern boundary results from a flow divergent pattern related to topography, as shown by point B in Figure 4. Each of these two boundaries was included in the model as no-flow boundaries. The northeast boundary is largely administrative as flow is parallel to the boundary (Yates et al. 2005). It was also modeled as a no-flow boundary. The western boundary is the sea, represented by a time-variable head boundary according to the imposed scenarios of sea-level rise. Two scenarios for sea level were considered: 0.5 m sea-level rise and 1 m sea-level rise. These scenarios were realized over a 100-year period (2006 to 2106), assuming a linear increase in the sea level over the period of analysis. The assumption of linear increase is supported by data presented in Nicholls and Cazenave (2010). The baseline sea level in 2006 equaled 0.903 m. This is the MSL in local reference to the NAVD88 vertical datum for 2006. Thus, the 0.5 and 1.0 m gains in sea level would bring the corresponding 2106 elevations to $(0.5 + 0.903 =) + 1.403$ m and $(1.0 + 0.903 =)1.903$ m, respectively. The total dissolved solid content (or salinity of average sea water) was set equal to 35,000 mg/L on the coastal boundary.

It was stated in the "Hydrogeology of the Seaside Area Sub-Basin" section that there are four formation units described in the aquifer system (Muir 1982; Yates et al. 2005). The surface of the top layer was generated from the National Elevation Dataset at a resolution of 1 arc second (USGS 2008). The positions of the bottoms of the four groundwater formations layer were estimated from cross sections presented in Muir (1982) and Yates et al. (2005). These cross sections were geo-referenced, and the layers' boundary surfaces were then interpolated

and extrapolated using the Matlab implementation of Sandwell's biharmonic spline algorithm (Sandwell 1987).

The FEFLOW model utilized a finite-element triangular mesh consisting of approximately 10,000 nodes on the top surface and on the bottom surface of each layer, where hydraulic head and groundwater salinity were calculated. The layout of the mesh of finite-element cells is shown in Figure 5 for the surface of the top layer. Each triangular element shown in Figure 5 extends from the top surface to the bottom surface of the four-layer Seaside Area aquifer system and it is segmented vertically into four parts, one for each of the four layers in the aquifer. The finite-element cells have a vertical dimension equal to the thickness of each layer, which varies depending of the locations of cells. The spatial dimension of the sides of the mesh triangles did not exceed 80 m. The spatial resolution of the triangular mesh was refined near the coast and wells to improve numerical accuracy near these features, as shown in Figure 5.

The 20 groundwater extraction wells referred in the section "Historical Groundwater Extraction in the Seaside Area Sub-Basin" plus two injection wells were used to model extraction and injection for the sub-basin. The extraction wells averaged 15,340 m^3/d of pumping in 2002 to 2006 (or 5.60×10^6 m^3 annually). The injection wells recharged on average 628 m^3/d in the period 2002 to 2006. The locations of the wells and their extraction or recharge rates were taken from Durbin (2007) and corroborated with Yates et al. (2005). The scenario for changed groundwater extraction during the 21st century input to FEFLOW was $Q = 15{,}340$ m^3/d. The baseline condition for groundwater extraction was chosen equal to the estimated safe yield, $Q_0 = 9730$ m^3/d (see section "Historical Groundwater Extraction in the Seaside Area Sub-Basin").

Aquifer Parameter Specification

Horizontal conductivity (K_{xy}) was assigned an initial value of 0.7 m/d. Vertical conductivity (K_z) was assigned an initial value of 0.3 m/d. These estimates underwent calibration to yield final values of hydraulic conductivity that were largely in line with those published by Yates et al. (2005). Storativity was assigned an initial value ranging between 0.1 and 0.15 (Muir 1982; CDWR 2003). Porosity was specified in the range 0.10 and 0.15, the lower values assigned to the deeper formations. Longitudinal dispersivity was assigned an initial value ranging 10 m, with the ratio of transversal to longitudinal dispersivity set equal to 0.10. The values of porosity and dispersivities were selected from a database by Waterloo Hydrogeologic Inc. (2000) that correlates these properties to lithology.

The chosen initial values of hydraulic conductivity, storage coefficient, recharge, and dispersivity underwent calibration. The assigned porosities (0.10 to 0.15) retained their values because adequate calibration was achieved by calibrating other parameters. Calibration for the Seaside numerical simulation model consisted of two phases. The first phase (pre-calibration) involved systematically varying the principal parameters: recharge, storage coefficient, and hydraulic conductivity until obtaining hydraulic heads that matched pre-extraction hydraulic head data presented in Muir (1982). Pre-extraction refers to year 1956 hydraulic head. The second calibration phase consisted of simulating hydraulic head and groundwater salinity in the period 1956 to 2006. The historical pumping and injection data for this phase were used in the numerical simulations of hydraulic head and sea water intrusion. During this phase, an attempt was made to meet three criteria. First, overall water levels were allowed to drop until they approximately matched the contours published in Muir (1982) and Yates et al. (2005) for 1979 and 2002, respectively. Second, the hydraulic head simulations were refined to replicate the cone of depression of a size and depth nearly equal to the one that currently surrounds the production wells in the northern coastal subarea. Third, the calibration simulations were refined so that no appreciable sea water intrusion occurred by the year 2006, consistent with field conditions. Net recharge, hydraulic conductivity, storage coefficient, and dispersivity were calibrated in the second phase until the criteria were met.

The final calibrated parameters were as follows: horizontal conductivity 0.5 to1.2 m/d, vertical conductivity 0.2 to 0.4 m/d, storage coefficient 0.11 to 0.13, recharge identical to the values given in the section "Hydrogeology of the Seaside Area Sub-Basin"; longitudinal dispersivity 10 m with a lateral dispersivity to longitudinal dispersivity ratio equal to 0.10.

Scenarios for Numerical Simulations of Sea Water Intrusion

The baseline condition was designated to correspond to year 2006, with assigned baseline groundwater extraction equal to $Q_0 = 15{,}340$ m^3/d and baseline sea level equal to $R_0 = 0.903$ m. The leading position of the 10,000 mg/L iso-salinity line in 2006 was approximately 0.170 km (170 m) landward measured from the coastline defined by the baseline sea level. The position of the 2006 coastline was kept constant for all the simulation scenarios that follow. This was necessary to keep comparisons among the locations of the 10,000 mg/L iso-salinity line resulting from different scenarios of sea-level rise tied to a unique baseline position of the coastline. For the range of sea-level rise considered (with a maximum 1 m rise over 100 years), it is reasonable to envision the construction of coastal barriers to contain coastal flooding by rising sea level. Several simulations of sea water intrusion were conducted for the period 2006 to 2106: Scenario I imposes post-development (i.e., post-2006) groundwater extraction ($Q = 15{,}340$ m^3/d) and 1.0 m sea-level rise between 2006 and 2106 ($R = 1.903$ m); scenario II sets $Q = 15{,}340$ m^3/d as done in scenario I but with 0.5 m sea-level rise between 2006 and 2106 ($R = 1.403$ m); scenario III uses baseline groundwater extraction $Q_0 = 9730$ m^3/d but with 0.1 m sea-level rise between 2006 and 2106 ($R = 1.903$ m); scenario IV sets baseline groundwater extraction $Q_0 = 9730$ m^3/d as done

Table 2
Summary of Simulation Scenarios

Simulation Scenario	Sea-Level Rise 2006–2106 (m)	Groundwater Extraction (m^3/d)
I (Equation 1)	1.0	Post-2006 = 15,340
II (Equation 1)	0.5	Post-2006 = 15,340
III (Equation 2)	1.0	Baseline = 9730
IV (Equation 2)	0.5	Baseline = 9730
V (Equation 3)	0.0	Post-2006 = 15,340

Note: The sea-level rise in the table must be added to the baseline sea-level in 2006 equal to $R_0 = 0.903$ m to obtain the year 2106 sea level.

in simulation scenario III but with 0.5 m sea-level rise between 2006 and 2106 ($R = 1.403$ m); scenario V poses post-development (i.e., post-2006) groundwater extraction ($Q = 15{,}340$ m^3/d) and baseline sea level between 2006 and 2106 ($R_0 = 0.903$ m). The five simulation scenarios are summarized in Table 2.

Simulations under scenarios I and II approximate Equation 1 (for total change caused by sea-level rise while groundwater extraction increases), whereby the former relies on 1.0 m sea-level rise, whereas the latter adopts 0.5 m sea-level rise. Simulations with scenarios III and IV approximate Equation 2 (for change caused by sea-level rise while groundwater extraction equals its baseline value), whereby the former prescribes a 1.0 m sea-level rise whereas the latter relies on a 0.5 m sea-level rise. Simulation under scenario V approximates Equation 3 (for change caused by increased groundwater extraction with sea level set at its baseline value). The results of the numerical simulations of sea water intrusion are discussed in the following section.

Results of the Numerical Simulations

Figure 6 shows the (vertically-averaged) hydraulic head for years 1956 (the pre-development condition), 2006 (showing the initial head distribution used in the simulations of sea water intrusion), and 2106 (showing the simulated head distribution). The 1956 head distribution showed an average hydraulic gradient across the East-West axis of the Seaside Area sub-basin (shown in Figure 4) close to 8.2/1000 that drove submarine discharge toward the ocean bottom prior to heightened groundwater extraction. By year 2006, the hydraulic head had developed a cone of depression in the area of largest groundwater extraction. The year-2106 head distribution was calculated with post-2006 groundwater extraction ($Q = 15{,}340$ m^3/d) and baseline sea level ($R_0 = 0.903$ m) or simulation scenario V. The 2106 head distribution exhibits a cone of depression near the major extraction wells in excess of −30 m. The effect of 21st-century groundwater extraction plays a key role in sea water intrusion, as shall be shown in the following paragraphs.

Figure 6. Simulated (vertically-averaged) hydraulic head distribution (in meters above North American Vertical Datum of 1988) assuming post-2006 net groundwater extraction rate ($Q = 15{,}340$ m^3/d) in the Seaside Area sub-basin. Sea level was maintained at the 2006 (baseline) level throughout the simulation ($R_0 = 0.903$ m). Notice the formation of a cone depression in excess of −30 m by 2106.

Figure 7 shows the simulated (vertically-averaged) salinity for year 2106 in the Seaside Area sub-basin under simulation scenario I, that is, assuming 1 m of sea-level rise ($R = 1.903$ m) and post-2006 groundwater extraction ($Q = 15{,}340$ m^3/d). It is seen in Figure 7 that the leading point of the 10,000 mg/L iso-salinity line lies about 760 m inland (measured from the coastline) in the area near the major production wells, while that of the 1000 mg/L iso-salinity line intruded about 1200 m in the same area. Simulations of salinity under scenario II, which corresponds to $Q = 15{,}340$ m^3/d and 0.5 m sea-level rise ($R = 1.403$ m), were also conducted. They resemble closely the salinity pattern shown in Figure 7, except that the leading points of the 10,000 and 1000 mg/L iso-salinity lines were approximately 750 and 1185 m from the coastline, respectively.

Figure 8 depicts on its left pane the simulated locations of the 1000 and 10,000 mg/L (vertically-averaged) iso-salinity lines in year 2106 assuming a 1 m rise in sea level during the 21st century ($R = 1.903$ m) and post-2006 groundwater extraction ($Q = 15{,}340$ m^3/d), that is, under simulation scenario I. Notice that the leading positions of the 10,000 and 1000 mg/L iso-salinity lines are located about 760 and 1200 m from the coastline,

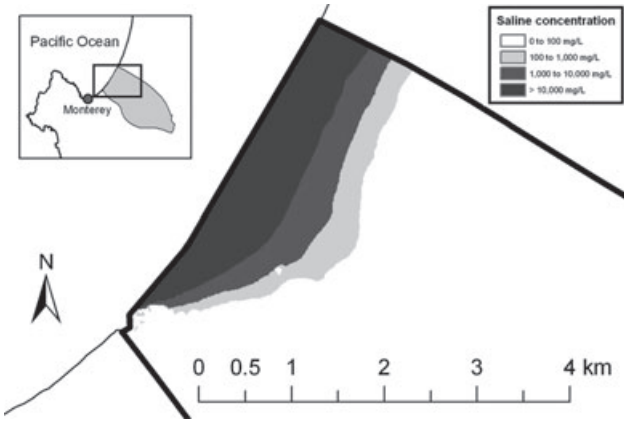

Figure 7. Simulated (vertically-averaged) salinity in the Seaside area sub-basin for year 2106 corresponding to simulation scenario I, or post-2006 groundwater extraction ($Q = 15{,}340$ m^3/d) and 1 m sea-level rise ($R = 1.903$ m).

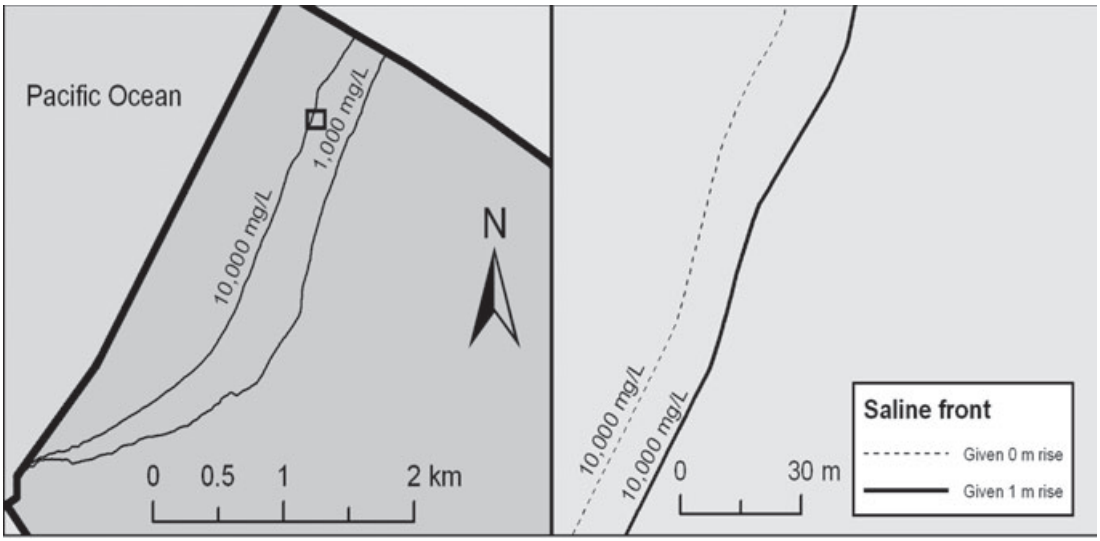

Figure 8. Simulated (vertically-averaged) iso-salinity lines. Left pane illustrates the locations of the 1000 and 10,000 mg/L iso-salinity lines for the year 2106 under scenario I (with post-2006 groundwater extraction, $Q = 15,340$ m^3/d, and 1 m sea-level rise, $R = 1.903$ m). The small squared area on the left pane's north-central region is zoomed in on the right pane. The right pane shows the difference between the calculated 10,000 mg/L iso-salinity lines under scenarios I and V. The latter scenario prescribes post-2006 groundwater extraction, $Q = 15,340$ m^3/d, and baseline sea level, $R_0 = 0.903$ m. Notice that the 10,000 mg/L iso-salinity line corresponding to the 1 m sea-level rise scenario is between 12 and 18 m farther inland than the iso-salinity line associated with the baseline sea level scenario.

respectively. The small squared area on the left pane's north-central region was zoomed in on the right pane of Figure 8. The right pane shows the difference between the calculated 10,000 mg/L iso-salinity lines under scenarios I and V. The latter scenario prescribes post-2006 groundwater extraction, $Q = 15,340$ m^3/d, and baseline sea level ($R_0 = 0.903$ m). Notice that by 2106, the 10,000 mg/L iso-salinity line corresponding to the 1 m sea-level rise scenario is between 12 and 18 m farther inland than the iso-salinity line associated with the baseline sea-level scenario.

Similar differences were calculated between the positions of the 10,000 mg/L iso-salinity line under scenario II, with $Q = 15,340$ m^3/d and 0.5 m sea-level rise, and scenario V. The small differences between simulated sea water intrusions corresponding to scenarios I (or II) and V established that groundwater extraction, instead of sea-level rise, is the predominant cause of sea water intrusion in this case. This assertion is confirmed by a comparison of the positions of the 10,000 mg/L iso-salinity front corresponding to simulation scenarios I ($Q = 15,340$ m^3/d, $R = 1.903$ m), III ($Q = 9730$ and $R = 1.903$ m), and V ($Q = 9730$ and $R_0 = 0.903$ m) shown in Figure 9. It is seen there that of the 760 m of total 10,000 mg/L iso-salinity advance, 745 m are contributed by the rise of groundwater extraction and 12 m are contributed by sea-level rise of 1 m over the 100-year period of analysis. The fact that the latter two contributions do not add exactly to 760 m is due to the fact that sea water intrusion is not driven exactly in a linear fashion by groundwater extraction and sea-level rise, a possibility stated in the section "Method for Assessing the Contributions of Sea-Level Rise and Groundwater Extraction to Sea Water Intrusion."

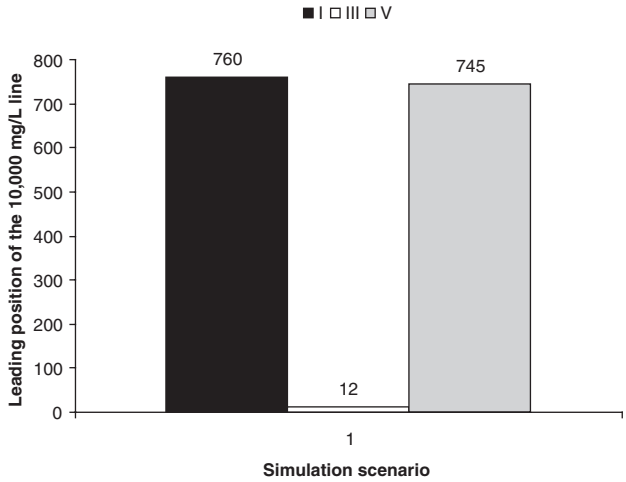

Figure 9. The leading position of the 10,000 mg/L iso-salinity line in year 2106 associated with simulation scenarios I, III, and V, listed in Table 2, is shown. Notice that the contribution to sea water intrusion of 1 m sea-level rise with baseline groundwater extraction (scenario III) is very small compared with scenarios I and V, both of which impose post-2006 groundwater extraction.

The dominance of groundwater extraction over sea-level rise in inducing sea water intrusion observed in Figure 9 is confirmed in Figure 10. The latter shows the positions of the 10,000 mg/L iso-salinity front corresponding to simulation scenarios II ($Q = 15,340$ m^3/d, $R = 1.403$ m), III ($Q = 9730$ and $R = 1.903$ m), and V ($Q = 9730$ and $R_0 = 0.903$ m) shown in Figure 10. It is seen there that of the 752 m of total 10,000 mg/L iso-salinity advance, 745 m are contributed by the rise of

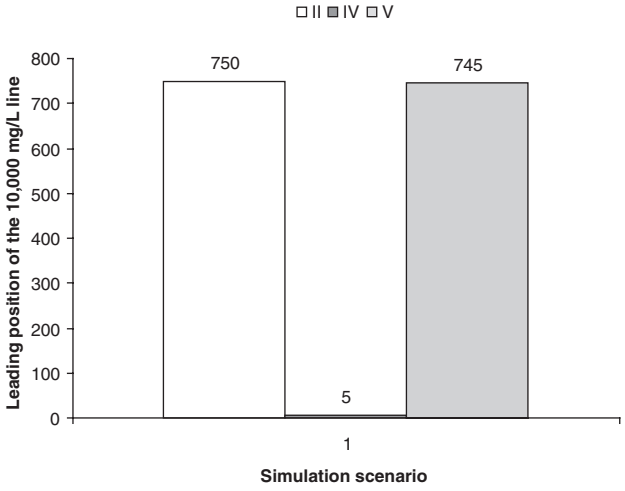

Figure 10. The leading position of the 10,000 mg/L isosalinity line in year 2106 associated with simulation scenarios II, IV, and V, listed in Table 2, is shown. Notice that the contribution to sea water intrusion of 0.5 m sea-level rise with baseline groundwater extraction (scenario IV) is very small compared with scenarios II and V, both of which impose post-2006 groundwater extraction.

groundwater extraction and 6 m are contributed by sea-level rise of 1 m over the 100-year period of analysis.

Summary and Conclusion

This article has presented a method to quantify the individual and total effects of sea-level rise and groundwater extraction on sea water intrusion in coastal aquifers. A mathematical formulation of the resolution of sea water intrusion among its causes was quantified via numerical simulation under three key scenarios of change in the 21st century, named herein scenarios I (post-2006 groundwater extraction and 1 m sea-level rise), III (baseline groundwater extraction and 1 m sea-level rise), and V (post-2006 groundwater extraction and baseline sea level). The method was illustrated with data and scenarios of sea-level rise and groundwater extraction in the Seaside Area groundwater sub-basin in Monterey County, California. The numerical model's results predict an expanded zone of sea water intrusion under scenario I on the order of 15 to 30 m approaching the coastal production wells compared to the sea water advance associated with scenario V over the next 100 years (2006 through 2106). The expanded zone of sea water intrusion advance was measured relative to the sea water intrusion caused by groundwater extraction without sea-level rise over the same period and it comprises saline concentrations of groundwater in the range 1000 to 10,000 mg/L. It is evident from our numerical simulations that groundwater extraction is the dominant factor in inducing sea water intrusion in the Seaside Area sub-basin. The vulnerability of other coastal aquifers to sea-level rise and groundwater extraction is the subject of continuing research, whose results will be reported at a later time.

Besides resolving the contributions of groundwater extraction and sea-level rise to sea water intrusion in the study aquifer, the method presented in this work is applicable to coastal aquifers under a variety of other scenarios of change not considered in this work. For example, one could resolve by skilled application of this article's method, what changes in groundwater extraction and/or sea-level would cause specified levels of groundwater salinization at strategic locations.

Acknowledgments

This project was made possible through grant SD017 from the University of California Water Resources Center. The authors also wish to thank management officials at the Monterey Peninsula Water Management District for providing clarifications and interpretations of existing reports on groundwater in their basins. Three reviewers and the Editor submitted insightful suggestions that improved our work.

References

Anderson, J., K. Miliken, and D. Wallace. 2010. Coastal impact underestimated from rapid sea level rise. *EOS, Transactions of the American Geophysical Union* 91, no. 23: 205–206.

Bachman, S., C. Hauge, R. McGlothlin, K. Neese, T. Parker, A. Saracino, and S. Slater. 2005. *California Groundwater Management,* 2nd ed., Sacramento, California: Groundwater Resources Association of California.

Barazzuoli, P., M. Nocchi, R. Rigati, and M. Salleolini. 2008. A conceptual and numerical model for groundwater management: A case study on a coastal aquifer in southern Tuscany, Italy. *Hydrogeology Journal* 16, no. 8: 1557–1576.

Bates, B., Z.W. Kundzewicz, S. Wu, and J. Palutikof, eds. 2008. *Climate Change and Water. Technical Paper of the Intergovernmental Panel on Climate Change.* Geneva, Switzerland: IPCC Secretariat.

Bear, J., A.H.-D. Cheng, S. Sorek, D. Ouzar, and I. Herrera. 1999. *Seawater Intrusion in Coastal Aquifers: Concepts, Methods, and Practice.* Dordrecht, The Netherlands: Kluwer Academic Publishers.

Bray, B., F.T. Tsai, Y. Sim, and W.W. Yeh. 2007. Model development and calibration of a saltwater intrusion model in Southern California. *Journal of the American Water Resources Association* 43, no. 5: 1329–1343.

California Department of Water Resources (CDWR). 2003. *California's Groundwater. Bulletin 118.* Sacramento, California.

California Department of Water Resources (CDWR). 2006. *Progress on Incorporating Climate Change into Management of California's Water Resources*. Sacramento, California.

California Department of Water Resources (CDWR). 2009. *California Water Plan Update*. Sacramento, California.

Diersch, H.J.G. 2006. *FEFLOW 5.3: Finite Element Subsurface Flow and Transport Simulation System User Manual Version 5.3.* Berlin, Germany: WASY GmbH Institute for Water Resources Planning and Systems Research.

Douglas, B.C. 1997. Global sea level rise: A redetermination. *Surveys in Geophysics* 18, no. 2–3: 279–292.

Durbin, T.J. 2007. *Groundwater Flow and Transport Model: Seaside Groundwater Basin. Monterey County, California*, 33: RBF Consulting.

Faye, S., I.N. Diop, S.C. Faye, D.G. Evans, M. Pfister, P. Maloszewski, and K.P. Seiler. 2001. Seawater intrusion in the Dakar (Senegal) confined aquifer: calibration and

testing of a 3D finite element model. In *New Approaches Characterizing Groundwater Flow*, eds. K. P. Seiler and S. Wohnlich, 1183–1186: Lisse, The Netherlands: Swets & Zeitlinger.

Fetter, C.W. 2001. *Applied Hydrogeology*, 4th ed. Upper Saddle River, New Jersy: Prentice Hall.

Fugro West Inc. 1997. *Hydrogeologic Assessment, Seaside Coastal Groundwater Subareas, Phase III Update.* Monterey County, California: Monterey Peninsula Water Management District.

Ghyben, B.W. 1888. *Nota in verband met de voorgenomen putboring nabij Amsterdam (Notes on the probable results of the proposed well drilling near Amsterdam)*, 8–22. The Hague, The Netherlands: Tijdschrift van het Koninklijk Institunt van Ingeniers.

Hanson, R.T., P. Martin, and K.M. Koczot. 2003. *Simulation of Ground-Water/Surface-Water Flow in the Santa Clara-Calleguas Basin, Ventura County, California.* Sacramento, California: U.S. Geological Survey.

Herzberg, A. 1901. Die Wasserversorgung einiger Nordseeb~ider (The water supply on parts of the North Sea coast in Germany). *Journal Gabeleucht ung und Wasserversorg ung* 44: 815–819 and 824–844.

Intergovernmental Panel on Climate Change (IPCC). 2001. Climate change 2001. *The Scientific Basis*, eds. J.T. Houghton, Y. Ding, D. J. Griggs, M. Noguer, P.J. van der Linden, X. Dai, K. Maskell, and C.A. Johnson. Cambridge, UK: Cambridge University Press.

Intergovernmental Panel on Climate Change (IPCC). 2007. Climate change 2007. *The Physical Science Basis*, eds. S. Solomon, D. Qin, M. Manning, M. Marquis, K. Averyt, M.M.B. Tignor, H. L. Miller, Jr., and Z. Chen. Cambridge: Cambridge University Press.

Kumar, C.P., A.G. Chacahadi, B.K. Purandara, S. Kumar, and R. Juyal. 2007. Modeling of seawater intrusion in coastal area of north Goa. *Water Digest* 2, no. 3: 80–83.

Langevin, C.D., and W. Guo. 2006. MODFLOW/MT3DMS-based simulation of variable-density groundwater flow and transport. *Ground Water* 44, no. 3: 339–351.

Loáiciga, H.A. 2003a. Climate change and ground water. *Annals of the Association of American Geographers* 93, no. 1: 30–41.

Loáiciga, H.A. 2003b. Sustainable ground-water exploitation. *International Geology Review* 44, no. 12, 1115–1121.

Loáiciga, H.A. 2006. Modern-age buildup of CO_2 and its effects on seawater acidity and salinity. *Geophysical Research Letters* 33, no. 10: L10605. DOI: 10.1029/2006GL026305

Loáiciga, H.A. 2007. Reply to Comment by Caldeira et al. 2007 on "Modern-age CO_2 and its effect on seawater acidity and salinity". *Geophysical Research Letters* 34: L18603. Doi:10.1029/2006GL027506

Loáiciga, H.A. 2008. Phreatic surface in island aquifers with regular geometry and time independent recharge and pumping. *Mathematical Geosciences* 40: 199–211.

Loáiciga, H.A., W-G. Yeh, and M. Ortega-Guerrero. 2006. A. probability density functions in the analysis of hydraulic conductivity data. *Journal of Hydrologic Engineering* 11, no. 5: 442–450.

Masterton, J.P., and S.P. Garabedian. 2007. Effects of sea-level rise on groundwater flow in a coastal aquifer system. *Ground Water* 45, no. 2: 209–217.

Muir, K.S. 1982. *Ground Water in the Seaside Area, Monterey County, California.* Water-Resources Investigations 82-10, 37: U.S. Geological Survey.

National Geodetic Survey (NGS). 2009. *Continuously Operating Reference Stations*. http://www.ngs.noaa.gov/CORS/ (accessed March 13, 2009).

National Oceanic and Atmospheric Administration (NOAA). 2009. *Sea Level Trends*. http://tidesandcurrents.noaa.gov/sltrends/sltrends.shtml (accessed March 13, 2009).

Nicholls, R.J., and A. Cazenave. 2010. Sea-level rise and its impacts on coastal zones. *Science* 328: 1517–1520.

Sandwell, D.T. 1987. Biharmonic Spline Interpolation of GOES-3 and SEASAT Altimeter Data. *Geophysical Research Letters* 14, no. 2: 139–142.

Sandoval, E. 2008. Written communication, May 13, 2008.

Trefrey, M.G., and C. Muffels. 2007. FEFLOW: A finite-element ground water flow and transport modeling tool. *Ground Water* 45, no. 5: 525–528.

United States Geological Survey (USGS). 2008. National Elevation Dataset. http://ned.usgs.gov (accessed February 25, 2008).

U.S. Environmental Protection Agency. 1976. *Quality Criteria for Water.* Washington, DC: U.S. Environmental Protection Agency.

Waterloo Hydrogeologic Inc. 2000. *Visual Modflow.* Waterloo, Ontario, Canada: Waterloo Hydrogeologic Inc.

Werner, A.D., and C.T. Simmons. 2009. Impact of sea-level rise on sea water intrusion in coastal aquifers. *Ground Water* 47, no. 2: 197–204.

Yates, E.B., M.B. Feeney, and L.I. Rosenberg. 2005. *Seaside Groundwater Basin: Update on Water Resource Conditions* 47. Monterey, California: Monterey Peninsula Water Management District.

Yeh, W.W., and B. Bray. 2006. *Modeling and Optimization of Seawater Intrusion Barriers in Southern California Coastal Plain* 41. University of California Water Resources Center.

Zektser, I.S., H.A. Loáiciga, and J. Wolf. 2005. Environmental impacts of groundwater overdraft: Selected case studies in the Southwestern United States. *Journal of Environmental Geology* 47, no. 3: 396–404.